Modeling and analysis of in-plane bending in fibrous reinforcements with rotation-free shell finite elements.

Quentin Steer, Julien Colmars, Naim Naouar, Philippe Boisse

International Journal of Solids and Structures

Modeling and analysis of in-plane bending in fibrous reinforcements with rotation-free shell finite elements.

--Manuscript Draft--

Manuscript Number:	IJSS-D-20-00865R2
Article Type:	Research paper
Keywords:	Fabrics/textiles; forming; Fibrous reinforcements; In-plane bending; Neighboring elements; rotation-free finite elements
Corresponding Author:	Julien Colmars, Ph.D Campus LyonTech La Doua - INSA Lyon VILLEURBANNE CEDEX, FRANCE
First Author:	Quentin Steer, Ph.D
Order of Authors:	Quentin Steer, Ph.D
	Julien Colmars, Ph.D
	Naim Naouar, Ph.D
	Philippe Boisse, Prof.
Abstract:	Simulations of the draping is currently based on membrane and out-of-plane bending stiffnesses of the composite textile reinforcements. In this article, an additional stiffness of in-plane bending of fibers is introduced. This stiffness gives rise to the appearance of transition zones in the deformation of fibrous reinforcements, which have been experimentally highlighted. Second gradient approaches have made it possible to model these phenomena in continuous medium and 3D finite element. In this article, the curvature of the fibers leading to in-plane deformation energy is calculated from the position of neighboring elements, using rotation-free shell elements. The result is an efficient approach that can be used to simulate the forming of textile reinforcements.

Graphical Abstract

Modeling and analysis of in-plane bending in fibrous reinforcements with rotation-free shell finite elements.

Quentin Steer, Julien Colmars, Naim Naouar, Philippe Boisse

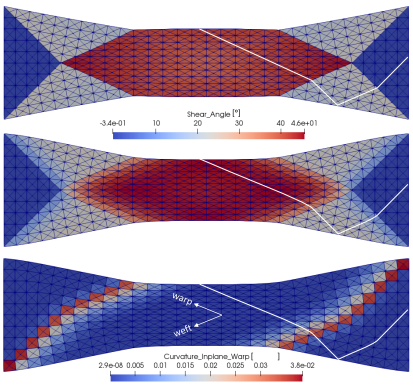

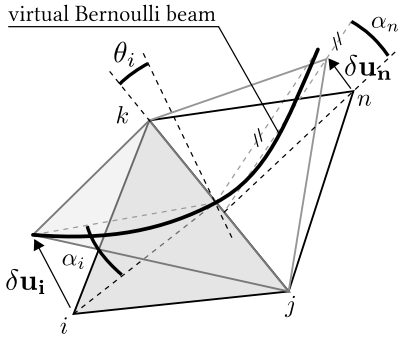

Highlights

Modeling and analysis of in-plane bending in fibrous reinforcements with rotation-free shell finite elements.

Quentin Steer, Julien Colmars, Naim Naouar, Philippe Boisse

- An energetical modeling is proposed in order to take into account in-plane bending of fibrous composite reinforcements, as an alternative to second gradient models.
- Enhancement of rotation free shell element for forming simulations was achieved, by taking into account in-plane bending energy.
- Unified approach for modeling in-plane and out of plane bending with rotation-free elements is obtained.

Modeling and analysis of in-plane bending in fibrous reinforcements with rotation-free shell finite elements.

Quentin Steer, Julien Colmars*, Naim Naouar, Philippe Boisse

Univ Lyon, INSA-Lyon, CNRS UMR5259, LaMCoS, F-69621, France

Abstract

Simulations of the draping is currently based on membrane and out-of-plane bending stiffnesses of the composite textile reinforcements. In this article, an additional stiffness of in-plane bending of fibers is introduced. This stiffness gives rise to the appearance of transition zones in the deformation of fibrous reinforcements, which have been experimentally highlighted. Second gradient approaches have made it possible to model these phenomena in continuous medium and 3D finite element. In this article, the curvature of the fibers leading to in-plane deformation energy is calculated from the position of neighboring elements, using rotation-free shell elements with explicit dynamic scheme. The result is an efficient approach that can be used to simulate the forming of textile reinforcements.

Keywords:

Fabrics/textiles, Forming, Fibrous reinforcements, In-plane bending, Neighboring elements, rotation-free finite elements

*Corresponding author

Email address: julien.colmars@insa-lyon.fr, +33 (0)4 72 43 82 48 (Julien Colmars)

1. Introduction

Composite materials make it possible to produce lighter structures thanks to their good mechanical characteristics in relation to their mass (Middendorf and Metzner, 2011; Meola et al., 2017). The combination of reinforcements and matrices are numerous and make it possible to adapt the composite to a given structure. On the other hand, the manufacture of defect-free composite parts is often complex. As a result, a major effort is being made to develop software for the simulation of manufacturing processes. In particular, the simulation of the forming of composite textile reinforcements is the subject of numerous developments (Gereke et al., 2013; Bussetta and Correia, 2018). This concerns the draping of dry reinforcements in LCM processes (Liquid Composite Molding) (Advani and Hsiao, 2012; Kruckenberg and Paton, 1998) which will be followed by the injection of the resin. Alternatively, forming concerns thermosetting prepregs (Lukaszewicz et al., 2012; Gangloff et al., 2014; Leutz et al., 2016; Sjölander et al., 2016; Alshahrani and Hojjati, 2017) or thermoplastic prepregs (Willems et al., 2008b,b; Harrison et al., 2013; Haanappel et al., 2014; Guzman-Maldonado et al., 2015; Dörr et al., 2017).

Modeling the forming of the fibrous reinforcement is a specific problem because its fibrous composition gives it a special mechanical behavior. Models for the simulation of the draping of reinforcements made of continuous fibers have been proposed in recent years. Kinematic drape modeling (also called pin-jointed net method (Wang et al., 1999; Potluri et al., 2001) or fishnet algorithm (Long and Rudd, 1994; Potluri et al., 2006, 2001; Hancock and Potter, 2006; Cherouat and Borouchaki, 2009) is the simplest approach that has been proposed for the simulation of draping. The method is purely

geometric, efficient and very fast numerically, but it does not take into account the nature of the reinforcement nor the boundary conditions in effort. Membrane approaches have been developed (Cherouat and Billot, 2001; Lin et al., 2007; ten Thije et al., 2007; Chen et al., 2015; Huang et al., 2020). The bending stiffness of fibrous fabrics being low, it is neglected in these models. So-called non-orthogonal (Xue et al., 2003; Yu et al., 2005a; Peng and Cao, 2005), hypoelastic (Khan et al., 2010) or hyperelastic (Holzapfel et al., 2004; Aimne et al., 2010) models are used to model the specificity of the behavior in the plane of the reinforcement. Nevertheless, it has been shown that bending stiffness, although low, plays an important role during draping in the onset and development of wrinkles (Boisse et al., 2011; Dangora et al., 2015). This is one of the most common defects in composite manufacturing (Skordos et al., 2007; Lightfoot et al., 2013; Hallander et al., 2015; Chen et al., 2016; Belnoue et al., 2018; Guzman-Maldonado et al., 2019).

Taking bending into account in draping simulations is not a simple issue. The possible slippage between the fibers makes the physics of textile reinforcement bending not correctly described by the classical plate bending theories of Kirchhoff and Mindlin. In these approaches, membrane stiffness and bending stiffness are related. In the case of fibrous reinforcements, they lead to much too great a bending stiffness. To avoid this difficulty, approaches have been developed that generally consist of decoupling the membrane strain and bending energies. The stress-resultant shell approaches relate membrane deformation to resulting membrane stresses on the one hand and bending to bending moments on the other (Hamila et al., 2009; Huang et al., 2020). Other approaches decouple member and bending stiffness by superimposing

finite elements, membrane and shell bending (e.g. DKT) (Haanappel et al., 2014; Dörr et al., 2018) or membrane and beam elements (Harrison et al., 2013; Dangora et al., 2015; Mitchell et al., 2016; Giorgio et al., 2018). Modifications of the properties in the thickness were also proposed in order to obtain the desired membrane stiffness and bending (Yu et al., 2005b; Gereke et al., 2013; Nishii et al., 2014; Dangora et al., 2015). A shell approach specific to fibrous reinforcements has also been proposed (Liang et al., 2017).

Beyond bending modeling, some aspects of the membrane behavior specific to fibrous reinforcements have been highlighted. In particular, the in-plane bending stiffness of fibers and yarns leads to transition zones when bending in the plane of the fibers (Fig.1-3). Second gradient approaches have made it possible to model these transition zones (Ferretti et al., 2014; Rahali et al., 2015; dellIsola and Steigmann, 2015; dAgostino et al., 2015; Boutin et al., 2017; Cuomo et al., 2017). Second gradient approaches make it possible to take into account the deformation energy related to the curvature in the plane of a fibrous reinforcement. Nevertheless, they are made in the framework of continuous modeling and the use of three-dimensional finite elements (or in plane stress if the problem is plane). Their implementation is not easy and the possibility of using them for the simulation of textile reinforcement draping is limited.

This article proposes to take into account a stiffness related to the in plane fiber curvature of a textile reinforcement. The calculation of the in plane curvature of this shell element uses the position of the neighboring elements. This technique was used for out-of-plane bending in rotation free finite elements developed for sheet metal forming (Oñate and Zárate, 2000;

Brunet and Sabourin, 2006). The method is here implemented using explicit dynamic scheme. It will be shown that the method leads to an efficient shell finite element that makes it possible to model transition zones in the analysis of textile reinforcements.

1.1. Strain modes of first gradient 3D models

Reinforcements can be thin or thick, but they generally have geometry that allows defining a mid-plane and a thickness; they can be independently modeled by shell or solid approaches. For this reason in the latter we call "membrane behavior" the material characteristics in the mid-plane, and transverse directions the directions perpendicular to the mid-plane.

For the forming simulation of woven reinforcements using solid elements, first gradient models have been developed at the yarn scale (Charmetant et al., 2011) and at the fabric scale (Charmetant et al., 2012). Hypoelastic (Khan et al., 2010) or hyperelastic (Charmetant et al., 2011, 2012) approaches has been developed for those models. In the case of hyperelastic approaches, strain energy W is written as the sum of decoupled strain modes. For example, in the case of (Charmetant et al., 2012) the energy density is written as :

$$W = W_\lambda + W_\gamma + W_\tau + W_\mu \tag{1}$$

where W_λ is the energy of tension in the fibers in the the warp and weft directions, W_γ the shear energy in the plane of the fabric (rotation of fibers directions), W_τ the transverse shear energy, and W_μ the compaction energy.In the membrane part of the behavior (warp-weft plane), the modes of tension

in the two fibers directions are by far the most rigid; they reflect the quasi-inextensibility of the carbon or glass fibers used in technical woven fabrics. This specificity of fibrous media is of the first order, even in geometrical simulations such as *fishnet algorithm*. The in-plane shear mode is also a determining factor, since it contributes to the drapability of the fabrics, i.e. its ability to be shaped on double-curvature geometries. Compression and transverse shear energies are important for thin (Nguyen et al., 2013) or thick fabrics to model thickness variations during compression in a mold or, for example, during the consolidation of thermoplastics.

1.2. Shell elements and enhanced first gradient models

Within the framework of forming simulations, many works have shown the importance of adding to the membrane or transverse part the out-of-plane bending stiffnesses in the directions of the fibers (Boisse et al., 2018; Hamila et al., 2009; Mathieu et al., 2015; Dörr et al., 2017), in order to adequately describe the formation of wrinkles. In fibrous media, the bending stiffness, which is often very low, cannot be directly deduced from the tensile stiffness (assumed to be infinitely rigid in the case of synthetic fibers), unlike in conventional continuous media. Many conventional solutions are decoupling the energy associated with tension and bending modes.

In shell models, the strain energy W is usually written :

$$W = W_\lambda + W_\gamma + W_\kappa \tag{2}$$

with W_κ the out-of-plane bending energy in both fiber directions.

1.3. Deformation modes for so-called second gradient models

The influence of second-gradient effects in fiber-reinforced hyper-elastic solids has been shown in (Spencer and Soldatos, 2007). The effects of fibers inextensibility was investigated in two-dimensional large deformation examples in (Soldatos, 2010).

Within the framework of 2^{nd} gradient solid elements applied to fibrous reinforcements (dellIsola and Steigmann, 2015; Madeo et al., 2015; Ferretti et al., 2014) the strain energy is written as the sum of a so-called first gradient energy W_I which depends on the transformation gradient $\mathbf{F}$ and a second gradient energy W_{II} which is also related to the gradient $\mathbf{F}$, such as :

$$W = W_I(\mathbf{F}) + W_{II}(\mathbf{F}, \nabla\mathbf{F}). \tag{3}$$

In these works, the shape of $W_I(\mathbf{F})$ is taken directly from the first gradient models proposed by (Charmetant et al., 2012). In the case of quasi-inextensible fibers, (dellIsola and Steigmann, 2015) shows that W_{II} can be written as a function of $\nabla\mathbf{F}$ only. Regarding the out-of-plane bending of the fibrous reinforcements, it has been shown that the shell models could give solutions close to solid models using second gradient (Boisse et al., 2018; Mathieu et al., 2015). The above-mentioned second gradient models are the only ones up to now that can also take into account the bending of the fibers in the plan. They were recently used to simulate standard forming cases with finite element (Barbagallo et al., 2017, 2019) but their use is still cost-effective due to high order shape functions.

Other approaches have been proposed to enhanced the membrane behavior of shell elements. The introduction of supplementary rotational degree of

freedom, named *drilling* DOFs, was described in (Hughes and Brezzi, 1989). Complete formulation of finite elements with *drilling* DOFs can be found in (Felippa, 2003; Shin and Lee, 2014). But to the best of our knowledge, no attempt was made to apply these methods to fibrous reinforcements.

1.4. Consideration of in-plane bending of the fibers

While out-of-plane bending has been adopted to describe more accurately the formation of wrinkles, in-plane bending of fibrous media has given rise to few developments, mainly based on generalized media models.

However, the in-plane bending of the fibers is a direct consequence of the presence of shear gradients in the woven fabrics, as the curvature is related to the second displacement gradient. In the case of inextensible fibers, the equivalence between bending energy and plane energy related to the shear gradient is shown in (Madeo et al., 2015).

The bending of the fibers in the plane has been observed experimentally. (Ferretti et al., 2014; Boisse et al., 2017) showed that taking into account the in-plane bending of the fibers modified the classical kinematics in the bias-extension test, introducing zones of shear gradients and curvature visible in Figure 1.

Tests conducted with the picture frame show that the fibers embedded in the frame are subjected to bending in the plane of the reinforcement (Willems et al., 2008a) ; which on an other hand explains the difficulty to avoid the occurrence of tensions in the direction of the fibers in this type of test.

Finally, it is possible to observe the bending of the fibers in the plane during the forming step of reinforcements (Tephany et al., 2016; Allaoui et al., 2014). In Figure 3 the in-plane bending of fibers when shaping a prism

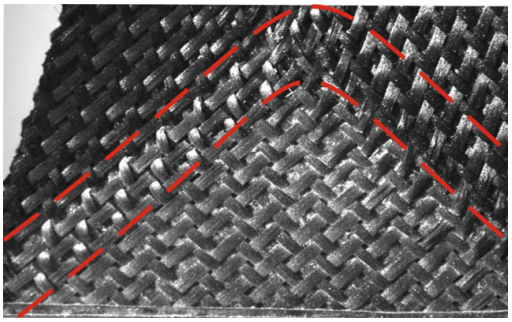

Figure 1: Transition zones in the bias extension test according to (Ferretti et al., 2014)

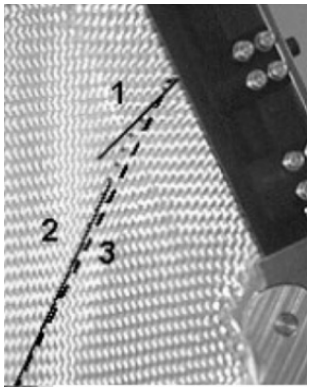

Figure 2: Bending of the fibers at embedding border in a picture frame test, after (Willems et al., 2008a)

is shown.

In this paper a shell approach able to take into account the membrane energy related to fibers in-plane bending (noted W_χ in the following) is proposed, based on the neighbor elements method. In this paper the shell energy of Equation 2 is extended to:

$$W = W_\lambda + W_\gamma + W_\kappa + W_\chi \tag{4}$$

First part of the paper will focus on the calculation of in-plane curvature.

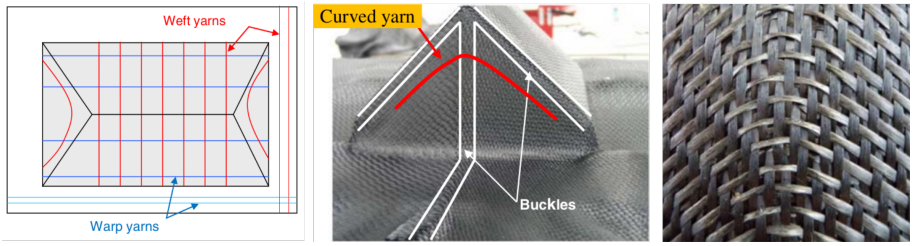

Figure 3: In-plane bending of fibers during a forming on a prism shape (Allaoui et al., 2014)

Complete constitutive equations and material parameters will be given in Section 3, then first simulations will be presented in Section 4.

We will show that such a shell formulation: enables to retrieve the results obtained by generalized continuum mechanics models; propose an alternative to shells with drilling DOFs; and account for new energy mode into finite elements that are already used for the forming of fibrous reinforcements.

2. Rotation free elements and neighbors elements

To model out-of-plane bending of fibrous reinforcements, several methods have been proposed for shells and solid elements. Some of them are based on shell elements without rotational degrees of freedom, and the curvature is then calculated by the neighbor elements method, as in (Hamila et al., 2009; Mathieu et al., 2015). Others are based on a decomposition of the stress tensor, into one part related to the membrane behavior, and a second part dedicated to the bending behavior (Dörr et al., 2017), according to the method of (Khan et al., 2010) for the membrane behavior. In the following we show that the neighboring element method can be used to calculate the membrane curvature as well.

2.1. Explicit dynamic approach

The following method was implemented in the framework of explicit dynamic approach, widely used for forming applications (Belytschko and Hughes, 1983). In the following, energies and kinematic variables (displacements, curvatures, shear angles, etc.) are calculated in their incremental form (noted with δ.) over small time steps; the increment are summed over time to account for large displacements.

2.2. Curvature calculation in rotation free elements

The element proposed by (Hamila et al., 2009) for woven modeling is based on the S3 element developed by (Sabourin and Vives, 2001; Sabourin and Brunet, 2006; Brunet and Sabourin, 2006). The rise of commercial calculation codes in the 1990s led to the development of finite elements with a relatively simple formulation and a limited number of degrees of freedom for sake of efficiency. The S3 element is part of a category of shell elements called *rotation free* like the BPT element developed by (Oñate and Zárate, 2000) or as developed in (Laurent and Rio, 2001). The S3 element is a triangular element with linear shape functions, having three degrees of freedom in translation at each node of the element. These elements are of particular interest for simulating the stamping of thin sheet metal. The out-of-plane curvature is calculated from the displacement of the nodes of neighboring elements.

According to the work of (Batoz and Gouri, 1990; Morley, 1971), the incremental curvature pseudo-vector $\{\delta\chi\}$ due to a virtual displacement can be calculated in a local orthogonal frame $(\mathbf{e_x}, \mathbf{e_y})$ from the rotation of fibers around the edges of the element over a time step :

$$\{\delta\chi\} = \begin{Bmatrix} \delta\chi_{xx} \\ \delta\chi_{yy} \\ 2\delta\chi_{xy} \end{Bmatrix} = - \begin{Bmatrix} \frac{\partial^2 w}{\partial x^2} \\ \frac{\partial^2 w}{\partial y^2} \\ 2\frac{\partial^2 w}{\partial xy} \end{Bmatrix} = - \sum_{i=1}^{3} \frac{2}{h_i} \begin{Bmatrix} -{c_i}^2 \\ -{s_i}^2 \\ 2c_i s_i \end{Bmatrix} \theta_i \tag{5}$$

$$c_i = \mathbf{n_i} \cdot \mathbf{e_x} \tag{6}$$

$$s_i = \mathbf{n_i} \cdot \mathbf{e_y} \tag{7}$$

with $\mathbf{n_i}, i = 1..3$ outgoing normal vectors at the edges of the elements (see Figure 4), w is the virtual displacement of fibers during a time step, and x and y the coordinates in the frame $\mathbf{e_x}, \mathbf{e_y}$. The angles θ_i represent the rotation of the fibers at the edges of the elements during a time step (Figure 5).

Equation 5 gives the curvatures in the element as used by (Hamila et al., 2009) to calculate the out-of-plane curvatures. It will be used here to calculate both out-of-plane and membrane curvatures ; the method for in-plane curvature differs from that of out-of-plane bending (Hamila et al., 2009) by the calculation of the angles θ_i, which is detailed in the following.

2.3. Calculation of the fibers rotations over a time step

Methods based on neighbor elements allow to calculate the angles θ_i from the incremental nodes displacements of the current element and its neighbors

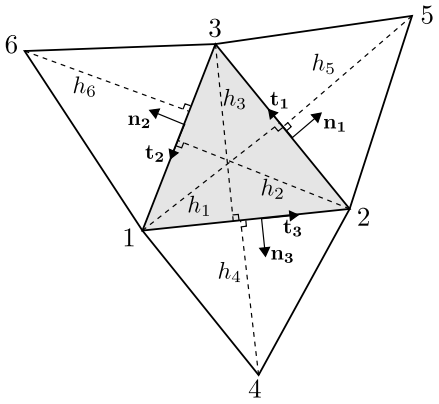

Figure 4: current element (gray) and its neighboring elements.

$\{\delta u\}_{18\times 1}$ (3 DOF per node). A matrix $[Q]$ is sought as :

$$\begin{Bmatrix} \theta_1 \\ \theta_2 \\ \theta_3 \end{Bmatrix} = [Q]_{3\times 18} \begin{Bmatrix} \{\delta u_1\} \\ \{\delta u_2\} \\ \{\delta u_3\} \\ \{\delta u_4\} \\ \{\delta u_5\} \\ \{\delta u_6\} \end{Bmatrix} \ , \ \{\delta u_{i=1..6}\} \begin{Bmatrix} \delta u_i^x \\ \delta u_i^y \\ \delta u_i^z \end{Bmatrix} \tag{8}$$

In the following, matrices are noted between brackets [.] while braces {.} are used for column vectors; for clarity, the dimensions of the matrices and vectors are also indicated.

The calculation of θ_i in the case of out-of-plane bending has given rise to several methods in the literature. (Oñate and Zárate, 2000) suggests to calculate the θ_i by averaging the rotations on either side of the edge of the element. In (Sabourin and Vives, 2001; Sabourin and Brunet, 2006),

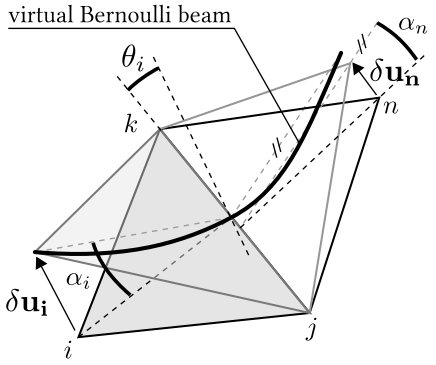

Figure 5: Fictive Bernouilli beam passing through the reference element and its neighbor, used for the calculation of the curvatures ; θ_i corresponds to the rotation of cross-section of the fictive beam at edge i.

the angles θ_i correspond to the cross-section rotations of a fictive Bernouilli beam passing through the vertices of the elements (Figure 5). This second approach is adapted here to the calculation of the curvature in the plane.

The calculation of rotations is similar to the method used for out-of-plane bending (Sabourin and Brunet, 2006). The angles θ_i can be written as a function of the angles α_i and α_n shown on Figure 5. During small time steps of explicit procedure (and small angles θ_i) we have:

$$\theta_i = \alpha_i \frac{h_i}{h_i + h_n} + \alpha_n \frac{h_n}{h_i + h_n} \tag{9}$$

with n the opposite node to i in the neighbor triangle (ex. for $i = 1$, $n = 5$).

Equation 9 can be written in matrix form :

$$\{\theta\}_{3\times1} = [G]_{3\times6} \{\alpha\}_{6\times1} \tag{10}$$

where the components of $[G]$ are directly obtained by Equation 9.

The angles $\alpha_i, i = 1..6$ are the rotations of the heights of the triangle and its neighbors. On the initial mesh, height direction $\mathbf{h}_i$ and length h_i are calculated from vertex i; it also gives point H_i position on edge $j-k$ (see Figure 6). Note that on initial mesh we have $\mathbf{h}_i = -\mathbf{n}_i$, but during the next steps, all vectors are updated and $\mathbf{h}_i$ is no longer collinear with $\mathbf{n}_i$ The α_i are decomposed into two terms, α_i^h and α_i^s which represent respectively the rotation of direction $\mathbf{h}_i$ with respect to the opposite side, and the rotation of the edge itself :

$$\alpha_i = \alpha_i^h - \alpha_i^s \tag{11}$$

This decomposition allows us to take into account the movement of rigid bodies α_i^s which is a methodological point that distinguishes membrane bending from out-of-plane bending.

The rotation α_i^h is finally written :

$$\alpha_i^h = \frac{\delta\mathbf{u}_i \cdot \mathbf{r}_i - \delta\mathbf{u}_{Hi} \cdot \mathbf{r}_i}{h_i} \tag{12}$$

with $\delta\mathbf{u}_i$ the displacement of node i, $\delta\mathbf{u}_{Hi}$ the displacement of point H_i (initial projection of vertex i on edge $j-k$); the displacement $\delta\mathbf{u}_{Hi}$ is interpolated from $\delta\mathbf{u}_j$ and $\delta\mathbf{u}_k$. The vector $\mathbf{r}_i$ is calculated form the vector product $\mathbf{r}_i = \mathbf{h}_i \times (\mathbf{n}_i \times \mathbf{t}_i)$.

The side rotation α_i^s is written :

$$\alpha_i^s = \frac{\delta\mathbf{u}_k \cdot \mathbf{n}_i - \delta\mathbf{u}_j \cdot \mathbf{n}_i}{L_i} \tag{13}$$

with $\delta\mathbf{u}_k$ and $\delta\mathbf{u}_j$ the incremental displacements of node j and k in the current triangle, and L_i the length of edge $j-k$. For example for the node $i = 1$ we get $k = 3$ and $j = 2$ (see Figure 4 and 6).

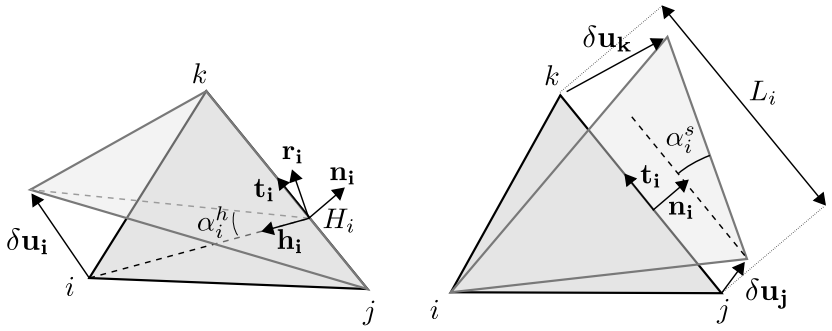

Figure 6: Definition of height rotations α_i^h (left), and edge rotations α_i^s (right) in the current elements.

We can write overall :

$$\{\alpha\}_{6\times1} = [H]_{6\times18}\,\{u\}_{18\times1} \tag{14}$$

The components of matrix $[H]$ should be computed from Equations 11-13.

By assembling equations (10) and (14) the rotations θ_i are finally obtained according to the displacements of the neighbor's nodes :

$$\{\theta\}_{3\times1} = [Q]_{3\times18}\,\{U\}_{18\times1} = [G]_{3\times6}\,[H]_{6\times18}\,\{U\}_{18\times1} \tag{15}$$

2.4. Bending boundary conditions

To take into account the boundary conditions, it is necessary to add an equation for the calculation of the fiber rotation. Next we give the equations corresponding to clamped or free edges. For these two cases, a virtual node f is created as the symmetrical of the node i with respect to the clamped edge -or respectively free edge- (see Figure 7).

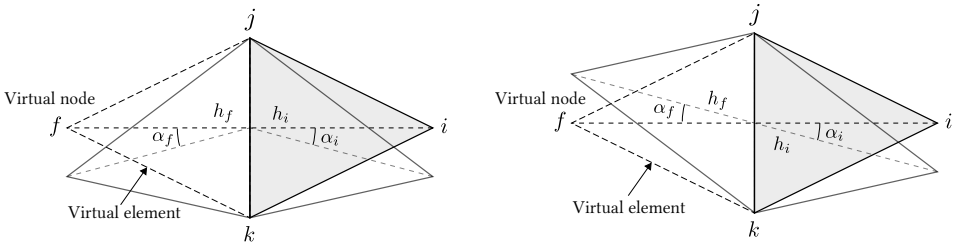

Figure 7: Virtual node f and virtual neighbouring element for boundary condition definition. (a) clamped edge and symmetry configurations, (b) free edge configurations.

In the case of clamped edge i (Figure 7a), $\alpha_i = -\alpha_f$, which is equivalent to postulate that the fiber does not rotate with respect to the clamped edge of the element, i.e. $\theta_i = 0$ according to Equation 9. Let's make two remarks about this :

- first, clamped edge condition is the same as the condition for an edge in a symmetry plane (from a beam point of view) since both conditions lead to $\theta_i = 0$;
- second, this does not necessarily imply zero curvature inside the element, since its value is calculated using θ_i on the three edges of the element (see Equation 5).

In the case of a free edge (Figure 7b) we simply get $\alpha_i = \alpha_f$, which leads to rotation of the fiber ($\theta_i \neq 0$).

3. In-plane bending energy and other deformation modes.

In-plane bending energy is written as a function of curvatures and integrated stresses :

$$\delta W_\chi = \int_S M_{11}^\chi \, \delta\chi_{11} + M_{22}^\chi \, \delta\chi_{22} \, \mathrm{d}S \tag{16}$$

$$M_{11}^\chi = k_1^\chi \chi_{11} \tag{17}$$

$$M_{22}^\chi = k_2^\chi \chi_{22} \tag{18}$$

where S is the area of the element, M_{11}^χ and M_{22}^χ are the moments of the integrated stresses in fiber directions $\mathbf{f_1}$ and $\mathbf{f_2}$, $\delta\chi_{11}$ and $\delta\chi_{22}$ are the curvatures in these two same directions. $\delta\chi_{11}$ and $\delta\chi_{22}$ are obtained by projection in both fiber directions of the complete in-plane curvature tensor $\boldsymbol{\delta\chi}$ (obtained in Equation 5).

$$\delta\chi_{11} = \boldsymbol{\delta\chi} : (\mathbf{f_1} \otimes \mathbf{f_1}) \tag{19}$$

$$\delta\chi_{22} = \boldsymbol{\delta\chi} : (\mathbf{f_2} \otimes \mathbf{f_2}) \tag{20}$$

The total bending energy is thus considered to be the addition of two independent non-orthogonal directions contributions. The bending energies of the two fiber directions will therefore be assumed to be decoupled. This hypothesis has been made in previous works on out-of-plane bending (Boisse et al., 2018), but coupling between bending rigidity of two fiber directions should be the subject of further experimental work.

In the following, it is assumed that the parameters of the behavior law are identical to those used for out-of-plane bending, resulting from the work

of (Abdul Ghafour et al., 2019) on a G1151 (Hexcel) reinforcement ; they are summarized in Table 1. The determination of in-plane bending specific properties must give rise to further experimental developments.

For the in-plane shear, the energy δW_γ is calculated by the following equations :

$$\delta W_\gamma = \int_S M^\gamma \, \delta\gamma \, \mathrm{d}S \tag{21}$$

$$M^\gamma = k_1^\gamma \gamma + k_3^\gamma \gamma^3 + k_5^\gamma \gamma^5 \tag{22}$$

where γ (and $\delta\gamma$) are the in-plane shear angle (or incremental shear angle), i.e. the angle variation between two fiber directions; M^γ is the associated shear moment. The calculation of $\delta\gamma$ is detailed in (Hamila et al., 2009). Out-of-plane bending is governed by the same equations as membrane bending (accounting for two independent fiber directions):

$$\delta W_\kappa = \int_S M_{11}^\kappa \, \delta\kappa_{11} + M_{22}^\kappa \, \delta\kappa_{22} \, \mathrm{d}S \tag{23}$$

$$M_{11}^\kappa = k_1^\kappa \kappa_{11} \tag{24}$$

$$M_{22}^\kappa = k_2^\kappa \kappa_{22} \tag{25}$$

On the other hand, the tension energy is calculated by the following equations :

$$\delta W_\lambda = \int_S F_{11}^\lambda \, \delta\lambda_{11} + F_{22}^\lambda \, \delta\lambda_{22} \, \mathrm{d}S \tag{26}$$

$$F_{11}^\lambda = k^\lambda \, \lambda_{11} \tag{27}$$

$$F_{22}^\lambda = k^\lambda \, \lambda_{22} \tag{28}$$

where F_{11} and F_{22} are the stress resultant for tension, and $\delta\lambda_{11}$ and $\delta\lambda_{22}$ the elongations in both fiber directions. Since the fibers are assumed to be quasi-inextensible, the k^{λ} parameter is taken large relative to the other parameters of the study.

In-plane bending			In-plane shearing			Out-plane bending		
k_1^{χ}	7.693	N.m^2	k_1^{γ}	1.00013	N.m^2	k_1^{κ}	7.693	N.m^2
k_2^{χ}	7.693	N.m^2	k_3^{γ}	-0.01939	N.m^4	k_2^{κ}	7.693	N.m^2
			k_5^{γ}	0.04160	N.m^6			
Tension			k^{λ}	1,000	N			

Table 1: G1151 properties from (Abdul Ghafour et al., 2019) used for the shell model.

4. Results

Membrane curvature calculation was implemented in PlasFib, a research finite element code using dynamic explicit scheme for forming simulation of composite reinforcements. Next we present simulations for material parameters presented in Table 1 obtained on a G1151 reinforcement.

4.1. Bias-extension-test

We present the simulation of a bias-extension test (BET) on a virtual 2D sample of size $240 \times 80\,\mathrm{mm}^2$. A displacement of about 46 mm was imposed at one end. On Figure 8 we show the results of two simulations, without and with taking into account the membrane bending (resp. Figure 8a and 8b). Figure 8a shows the classical first gradient solution based on inextensible

fibers; it exhibits three shearing zones (central maximal shear zone, half shear zone, and non-shearing zone near to the boundary conditions). The same solution can be obtain with a fishnet algorithm.

The second simulation with membrane bending exhibit the same zones, but with additional transition zones, which correspond to shearing gradients. These are the same transition zones as shown experimentally on Figure 1; the same qualitative results have been obtained using second gradient models (Ferretti et al., 2014).

On Figure 9 we show the shear angle and curvature fields along the M-N-P path of Figure 8, for both simulations (with and without membrane bending). Note that curvature is here given in weft direction along M-N segment while it is given in warp direction along N-P segment. Differences between the two simulations are put into evidence: the mean value of shearing angle is diminished when taking into account the in-plane bending energy. The resulting difference is a few degrees for the chosen material parameters. The shear distribution found with in-plane bending energy is in good accordance with the results of (Ferretti et al., 2014): along M-N segment the shear reaches a maximum of about 22 degree and then slightly decreses, while along N-P segment it reaches a maximum of about 42 degree before dropping slighlty towards 40 degrees.

As demonstrated in (Madeo et al., 2015; dellIsola and Steigmann, 2015), the shear gradient are related to in-plane bending. Figure 9 shows that curvature occurs in shear gradient zones.

In order to investigate the influence of mesh size, all simulations were performed with different meshes. In the case of BET simulation we used

three meshes of 1200, 4800 and 10800 elements. The evolution of curvature along M-N-P path for these three meshes is plot on Figure 10. Although we use a non local method (neighboring elements method), the method converges with the number of elements. The influence of mesh size is mainly visible in the transition zones, on both shear angle and curvature, while its influence in the other zones seems to be negligible. For better visualization the results of Figure 11a were plot only with 1200 elements.

4.2. Picture frame test

A picture frame test was simulated on a virtual specimen of size $240 \times 240\,\mathrm{mm}^2$ (Figure 11a). As in many experimental devices described in literature, fibers are clamped in the frame (Willems et al., 2008a); in the simulation displacements DOFs are linked to the frame while rotation of fibers is prevented by boundary conditions detailed in previous section.

Simulation results are presented on Figure 11a; it shows local shearing gradient (and curvature) next to the frame where fibers are clamped. In this case the solution of picture frame is not a constant shear zone anymore, although the central shearing remains the same (54.4°, see Figure 11b). Next to the clamped conditions we observe a $\pm 2°$ variation in shear angle. This oscillation of shear angle has to be related to local curvature gradients (the curvature locally increases and decreases from boundary to the center). The same phenomenon was observed numerically in the transition zones of the BET, both by our model and second gradient model by (Ferretti et al., 2014).

Figure 11c shows the evolution in time of tension, shearing and bending contributions to the total energy; this is done for both simulations, with and without in-plane bending rigidity. In this case the shearing energy is not

much affected by the addition of bending rigidity. Yet the bending rigidity results in a significant additional energy (40% of shearing energy) for the chosen parameters.

4.3. Cantilever test

In the last simulation example we use our in-plane bending model for unconventional application. We use it to perform a 2D simulation of cantilever bending test on a thick reinforcement. Here the displacements occur in the transverse plane of the reinforcement; thus finite elements are placed in the transverse plane, and not in the mid-plane anymore. The curvature χ, previously called in-plane curvature, will now stand for out-of-plane curvature of the sample. The sample is clamped on the left side, and a prescribed displacement is given at the other end. The mesh is visible on Figure 12a.

Figure 12a and 12b show the respective influence of bending or shearing parameters for a given shearing (resp. bending) rigidity. For the sake of clarity, all rigidity are considered linear ($k_3^\gamma = k_5^\gamma = 0$) while the parameters k_1^γ and k_1^χ are taken in a log scale: $k^\chi \in [1., 1000.]$N and $k_1^\gamma \in [0.1, 100]$N.mm^{-1}.

The method presented in this work allows decoupling the transverse shearing rigidity and the out-of-plane bending property, although the curvature is still related to shearing gradients. On Figure 12a we can see that the increasing bending rigidity does not affect the cross section rotation, while increasing k^γ directly modifies their orientation. For instance, for high transverse shearing rigidity, the model tends to a classical Bernoulli beam solution, where cross sections remain perpendicular to to mid-line.

The same test was conducted experimentally. It was performed on a thick interlock sample with dimensions $17 \times 50 \times 150$ mm. A 500 g dead

weight was hung to the right end. Small dots were painted on the sample in order to track the cross sections (Figure 13a). The experimental shape was in accordance with simulations with high k^χ/k^γ ratio (see Figure 12a).

Supplementary simulations were conducted in 3D with solid elements coupled with shells; the method used here was presented in details in (Mathieu et al., 2015) and consist of adding local bending stiffness using additional triangular rotation-free elements. Figure 13b shows the result of cantilever test with a first gradient hyperelastic model with parameters taken from (Charmetant et al., 2012), and Figure 13c shows the solution with additional bending rigidity. All simulations were conducted with PlasFib using dynamic explicit scheme.

The first gradient solution is consistent with our previous simulations with low bending rigidity (Figure 12a), while the second simulation is consistent with experimental solution and shapes of Figure 12a with higher bending rigidity.

5. Conclusion

In this paper we proposed a new solution for the modeling of in-plane bending in shells, with application to in-plane and out-of-plane bending in composite reinforcements. Neighboring element method used in previous studies for modeling out-of-plane bending was successfully adapted for modeling in-plane bending. It allowed reproducing complex kinematics of second gradient models found in the literature. This method revealed itself an efficient alternative to second gradient solutions which implies high interpolation finite element and thus are cost-effective in the context of forming simula-

tions. It is also an alternative method to the addition of drilling degree of freedom in shell elements. This work now raises the need of experimental developments in order to characterize the specific in-plane bending behavior of reinforcements.

This work is finally a contribution to the enhancement of rotation-free shell element for forming simulation, by taking into account in-plane bending energy. Neighboring element method can now be seen as a unified approach for both in-plane and out-of plane bending. The performance of such element was shown on classical fiber reinforcement characterization tests (bias extension test and picture frame test) and will be demonstrated on forming simulations in the near future.

References

Abdul Ghafour, T., Colmars, J., Boisse, P., 2019. The importance of taking into account behavior irreversibilities when simulating the forming of textile composite reinforcements. Composites Part A: Applied Science and Manufacturing 127, 105641. URL: https://linkinghub.elsevier.com/retrieve/pii/S1359835X19303902, doi:10.1016/j.compositesa.2019.105641.

Advani, S.G., Hsiao, K.T. (Eds.), 2012. Manufacturing techniques for polymer matrix composites (PMCs). Woodhead Publishing. doi:https://doi.org/10.1533/9780857096258.frontmatter.

Aimne, Y., Vidal-Sall, E., Hagge, B., Sidoroff, F., Boisse, P., 2010. A Hyperelastic Approach for Composite Reinforcement Large Deformation

Analysis. Journal of Composite Materials 44, 5–26. URL: http://journals.sagepub.com/doi/10.1177/0021998309345348, doi:10.1177/0021998309345348.

Allaoui, S., Hivet, G., Soulat, D., Wendling, A., Ouagne, P., Chatel, S., 2014. Experimental preforming of highly double curved shapes with a case corner using an interlock reinforcement. International Journal of Material Forming 7, 155–165. URL: http://link.springer.com/10.1007/s12289-012-1116-5, doi:10.1007/s12289-012-1116-5.

Alshahrani, H., Hojjati, M., 2017. Experimental and numerical investigations on formability of out-of-autoclave thermoset prepreg using a double diaphragm process. Composites Part A: Applied Science and Manufacturing 101, 199–214. URL: https://linkinghub.elsevier.com/retrieve/pii/S1359835X17302464, doi:10.1016/j.compositesa.2017.06.021.

Barbagallo, G., dAgostino, M.V., Aivaliotis, A., Daouadji, A., Makradi, A., Giunta, G., Boisse, P., Belouettar, S., Madeo, A., 2019. Model reduction for the forming process of fibrous composites structures via second gradient enriched continuum models. Mechanics of Advanced Materials and Structures 0, 1–12. URL: https://doi.org/10.1080/15376494.2019.1629050, doi:10.1080/15376494.2019.1629050, arXiv:https://doi.org/10.1080/15376494.2019.1629050.

Barbagallo, G., Madeo, A., Morestin, F., Boisse, P., 2017. Modelling the deep drawing of a 3D woven fabric with a second gradient model. Mathematics and Mechanics of Solids 22, 2165

– 2179. URL: https://hal.archives-ouvertes.fr/hal-01719711, doi:10.1177/1081286516663999.

Batoz, J.L., Gouri, D., 1990. Modlisation des structures par lments finis: poutres et plaques. volume 2. Hermes ed., Hermes.

Belnoue, J.P.H., Nixon-Pearson, O.J., Thompson, A.J., Ivanov, D.S., Potter, K.D., Hallett, S.R., 2018. Consolidation-Driven Defect Generation in Thick Composite Parts. Journal of Manufacturing Science and Engineering 140. URL: https://asmedigitalcollection.asme.org/manufacturingscience/article/doi/10.1115/1.4039555/473214/ConsolidationDriven-Defect-Generation-in-Thick, doi:10.1115/1.4039555.

Belytschko, T., Hughes, T.J., 1983. Computational methods for transient analysis. Amsterdam, North-Holland(Computational Methods in Mechanics. 1.

Boisse, P., Colmars, J., Hamila, N., Naouar, N., Steer, Q., 2018. Bending and wrinkling of composite fiber preforms and prepregs. A review and new developments in the draping simulations. Composites Part B: Engineering 141, 234–249. URL: https://linkinghub.elsevier.com/retrieve/pii/S1359836817340106, doi:10.1016/j.compositesb.2017.12.061.

Boisse, P., Hamila, N., Guzman-Maldonado, E., Madeo, A., Hivet, G., dellIsola, F., 2017. The bias-extension test for the analysis of in-plane shear properties of textile composite reinforcements and prepregs: a review. International Journal of Material Forming 10, 473–

492. URL: http://link.springer.com/10.1007/s12289-016-1294-7, doi:10.1007/s12289-016-1294-7.

Boisse, P., Hamila, N., Vidal-Sall, E., Dumont, F., 2011. Simulation of wrinkling during textile composite reinforcement forming. Influence of tensile, in-plane shear and bending stiffnesses. Composites Science and Technology 71, 683–692. URL: https://linkinghub.elsevier.com/retrieve/pii/S026635381100039X, doi:10.1016/j.compscitech.2011.01.011.

Boutin, C., dellIsola, F., Giorgio, I., Placidi, L., 2017. Linear pantographic sheets: Asymptotic micro-macro models identification. Mathematics and Mechanics of Complex Systems 5, 127–162. URL: http://msp.org/memocs/2017/5-2/p02.xhtml, doi:10.2140/memocs.2017.5.127.

Brunet, M., Sabourin, F., 2006. Analysis of a rotation-free 4-node shell element. International Journal for Numerical Methods in Engineering 66, 1483–1510. URL: http://onlinelibrary.wiley.com/doi/abs/10.1002/nme.1608, doi:10.1002/nme.1608.

Bussetta, P., Correia, N., 2018. Numerical forming of continuous fibre reinforced composite material: A review. Composites Part A: Applied Science and Manufacturing 113, 12–31. URL: https://linkinghub.elsevier.com/retrieve/pii/S1359835X18302732, doi:10.1016/j.compositesa.2018.07.010.

Charmetant, A., Orliac, J., Vidal-Sall, E., Boisse, P., 2012. Hyperelastic model for large deformation analyses of 3D interlock composite preforms. Composites Science and Technology 72, 1352–1360. URL: https://

linkinghub.elsevier.com/retrieve/pii/S0266353812001790, doi:10.1016/j.compscitech.2012.05.006.

Charmetant, A., Vidal-Sall, E., Boisse, P., 2011. Hyperelastic modelling for mesoscopic analyses of composite reinforcements. Composites Science and Technology 71, 1623–1631. URL: https://linkinghub.elsevier.com/retrieve/pii/S0266353811002351, doi:10.1016/j.compscitech.2011.07.004.

Chen, S., Harper, L., Endruweit, A., Warrior, N., 2015. Formability optimisation of fabric preforms by controlling material draw-in through in-plane constraints. Composites Part A: Applied Science and Manufacturing 76, 10–19. URL: https://linkinghub.elsevier.com/retrieve/pii/S1359835X15001608, doi:10.1016/j.compositesa.2015.05.006.

Chen, S., McGregor, O., Harper, L., Endruweit, A., Warrior, N., 2016. Defect formation during preforming of a bi-axial non-crimp fabric with a pillar stitch pattern. Composites Part A: Applied Science and Manufacturing 91, 156–167. URL: https://linkinghub.elsevier.com/retrieve/pii/S1359835X16303219, doi:10.1016/j.compositesa.2016.09.016.

Cherouat, A., Billot, J.L., 2001. Mechanical and numerical modelling of composite manufacturing processes deep-drawing and laying-up of thin pre-impregnated woven fabrics. Journal of Materials Processing Technology 118, 460–471. URL: https://linkinghub.elsevier.com/retrieve/pii/S0924013601009876, doi:10.1016/S0924-0136(01)00987-6.

Cherouat, A., Borouchaki, H., 2009. Present State of the Art of Composite

Fabric Forming: Geometrical and Mechanical Approaches. Materials 2, 1835–1857. URL: http://www.mdpi.com/1996-1944/2/4/1835, doi:10.3390/ma2041835.

Cuomo, M., dellIsola, F., Greco, L., Rizzi, N., 2017. First versus second gradient energies for planar sheets with two families of inextensible fibres: Investigation on deformation boundary layers, discontinuities and geometrical instabilities. Composites Part B: Engineering 115, 423–448. URL: https://linkinghub.elsevier.com/retrieve/pii/S1359836816318200, doi:10.1016/j.compositesb.2016.08.043.

Dangora, L.M., Mitchell, C.J., Sherwood, J.A., 2015. Predictive model for the detection of out-of-plane defects formed during textile-composite manufacture. Composites Part A: Applied Science and Manufacturing 78, 102–112. URL: https://linkinghub.elsevier.com/retrieve/pii/S1359835X15002432, doi:10.1016/j.compositesa.2015.07.011.

dellIsola, F., Steigmann, D., 2015. A Two-Dimensional Gradient-Elasticity Theory for Woven Fabrics. Journal of Elasticity 118, 113–125. URL: http://link.springer.com/10.1007/s10659-014-9478-1, doi:10.1007/s10659-014-9478-1.

Dörr, D., Henning, F., Kärger, L., 2018. Nonlinear hyperviscoelastic modelling of intra-ply deformation behaviour in finite element forming simulation of continuously fibre-reinforced thermoplastics. Composites Part A: Applied Science and Manufacturing 109, 585–596. URL: https://linkinghub.elsevier.com/retrieve/pii/S1359835X18301398, doi:10.1016/j.compositesa.2018.03.037.

Dörr, D., Schirmaier, F.J., Henning, F., Krger, L., 2017. A viscoelastic approach for modeling bending behavior in finite element forming simulation of continuously fiber reinforced composites. Composites Part A: Applied Science and Manufacturing 94, 113–123. URL: https://linkinghub.elsevier.com/retrieve/pii/S1359835X16304213, doi:10.1016/j.compositesa.2016.11.027.

dAgostino, M., Giorgio, I., Greco, L., Madeo, A., Boisse, P., 2015. Continuum and discrete models for structures including (quasi-) inextensible elasticae with a view to the design and modeling of composite reinforcements. International Journal of Solids and Structures 59, 1–17. URL: https://linkinghub.elsevier.com/retrieve/pii/S002076831400482X, doi:10.1016/j.ijsolstr.2014.12.014.

Felippa, C.A., 2003. A study of optimal membrane triangles with drilling freedoms. Computer Methods in Applied Mechanics and Engineering 192, 2125–2168. URL: https://linkinghub.elsevier.com/retrieve/pii/S0045782503002536, doi:10.1016/S0045-7825(03)00253-6.

Ferretti, M., Madeo, A., dellIsola, F., Boisse, P., 2014. Modeling the onset of shear boundary layers in fibrous composite reinforcements by second-gradient theory. Zeitschrift fr angewandte Mathematik und Physik 65, 587–612. URL: http://link.springer.com/10.1007/s00033-013-0347-8, doi:10.1007/s00033-013-0347-8.

Gangloff, J.J., Simacek, P., Sinha, S., Advani, S.G., 2014. A process model for the compaction and saturation of partially impregnated thermoset prepreg tapes. Composites Part A: Applied Science and Manufacturing

64, 234–244. URL: https://linkinghub.elsevier.com/retrieve/pii/S1359835X14001456, doi:10.1016/j.compositesa.2014.05.010.

Gereke, T., Döbrich, O., Hbner, M., Cherif, C., 2013. Experimental and computational composite textile reinforcement forming: A review. Composites Part A: Applied Science and Manufacturing 46, 1–10. URL: https://linkinghub.elsevier.com/retrieve/pii/S1359835X12003211, doi:10.1016/j.compositesa.2012.10.004.

Giorgio, I., Harrison, P., dell'Isola, F., Alsayednoor, J., Turco, E., 2018. Wrinkling in engineering fabrics: a comparison between two different comprehensive modelling approaches. Proceedings of the Royal Society A: Mathematical, Physical and Engineering Sciences 474, 20180063. URL: https://royalsocietypublishing.org/doi/10.1098/rspa.2018.0063, doi:10.1098/rspa.2018.0063.

Guzman-Maldonado, E., Hamila, N., Boisse, P., Bikard, J., 2015. Thermomechanical analysis, modelling and simulation of the forming of pre-impregnated thermoplastics composites. Composites Part A: Applied Science and Manufacturing 78, 211–222. URL: https://linkinghub.elsevier.com/retrieve/pii/S1359835X15002882, doi:10.1016/j.compositesa.2015.08.017.

Guzman-Maldonado, E., Wang, P., Hamila, N., Boisse, P., 2019. Experimental and numerical analysis of wrinkling during forming of multi-layered textile composites. Composite Structures 208, 213–223. URL: https://linkinghub.elsevier.com/retrieve/pii/S0263822318314326, doi:10.1016/j.compstruct.2018.10.018.

Haanappel, S., ten Thije, R., Sachs, U., Rietman, B., Akkerman, R., 2014. Formability analyses of uni-directional and textile reinforced thermoplastics. Composites Part A: Applied Science and Manufacturing 56, 80–92. URL: https://linkinghub.elsevier.com/retrieve/pii/S1359835X13002601, doi:10.1016/j.compositesa.2013.09.009.

Hallander, P., Sjölander, J., kermo, M., 2015. Forming induced wrinkling of composite laminates with mixed ply material properties; an experimental study. Composites Part A: Applied Science and Manufacturing 78, 234–245. URL: https://linkinghub.elsevier.com/retrieve/pii/S1359835X15002961, doi:10.1016/j.compositesa.2015.08.025.

Hamila, N., Boisse, P., Sabourin, F., Brunet, M., 2009. A semi-discrete shell finite element for textile composite reinforcement forming simulation. International Journal for Numerical Methods in Engineering 79, 1443–1466. URL: http://doi.wiley.com/10.1002/nme.2625, doi:10.1002/nme.2625.

Hancock, S., Potter, K., 2006. The use of kinematic drape modelling to inform the hand lay-up of complex composite components using woven reinforcements. Composites Part A: Applied Science and Manufacturing 37, 413–422. URL: https://linkinghub.elsevier.com/retrieve/pii/S1359835X05002356, doi:10.1016/j.compositesa.2005.05.044.

Harrison, P., Gomes, R., Curado-Correia, N., 2013. Press forming a 0/90 cross-ply advanced thermoplastic composite using the double-dome benchmark geometry. Composites Part A: Applied Science and Manufacturing

54, 56–69. URL: https://linkinghub.elsevier.com/retrieve/pii/S1359835X13001747, doi:10.1016/j.compositesa.2013.06.014.

Holzapfel, G.A., Gasser, T.C., Ogden, R.W., 2004. A new Constitutive Framework for Arterial Wall Mechanics and a Comparative Study of Material Models, in: Cowin, S.C., Humphrey, J.D. (Eds.), Cardiovascular Soft Tissue Mechanics. Kluwer Academic Publishers, Dordrecht, pp. 1–48. URL: http://link.springer.com/10.1007/0-306-48389-0_1, doi:10.1007/0-306-48389-0_1.

Huang, J., Boisse, P., Hamila, N., Zhu, Y., 2020. Simulation of Wrinkling during Bending of Composite Reinforcement Laminates. Materials 13, 2374. URL: https://www.mdpi.com/1996-1944/13/10/2374, doi:10.3390/ma13102374.

Hughes, T.J.R., Brezzi, F., 1989. On drilling degrees of freedom. Computer Methods in Applied Mechanics and Engineering 72, 105–121. URL: http://www.sciencedirect.com/science/article/pii/0045782589901242, doi:10.1016/0045-7825(89)90124-2.

Khan, M., Mabrouki, T., Vidal-Sall, E., Boisse, P., 2010. Numerical and experimental analyses of woven composite reinforcement forming using a hypoelastic behaviour. Application to the double dome benchmark. Journal of Materials Processing Technology 210, 378–388. URL: https://linkinghub.elsevier.com/retrieve/pii/S0924013609003598, doi:10.1016/j.jmatprotec.2009.09.027.

Kruckenberg, T., Paton, R. (Eds.), 1998. Resin Transfer Mould-

ing for Aerospace Structures. Springer Netherlands. URL: https://www.springer.com/gp/book/9780412731501, doi:10.1007/978-94-011-4437-7.

Laurent, H., Rio, G., 2001. Formulation of a thin shell finite element with continuity C0 and convected material frame notion. Computational Mechanics 27, 218–232. URL: http://link.springer.com/10.1007/s004660100243, doi:10.1007/s004660100243.

Leutz, D., Vermilyea, M., Bel, S., Hinterhölzl, R., 2016. Forming Simulation of Thick AFP Laminates and Comparison with Live CT Imaging. Applied Composite Materials 23, 583–600. URL: http://link.springer.com/10.1007/s10443-016-9475-6, doi:10.1007/s10443-016-9475-6.

Liang, B., Colmars, J., Boisse, P., 2017. A shell formulation for fibrous reinforcement forming simulations. Composites Part A: Applied Science and Manufacturing 100, 81–96. URL: https://linkinghub.elsevier.com/retrieve/pii/S1359835X17301744, doi:10.1016/j.compositesa.2017.04.024.

Lightfoot, J.S., Wisnom, M.R., Potter, K., 2013. A new mechanism for the formation of ply wrinkles due to shear between plies. Composites Part A: Applied Science and Manufacturing 49, 139–147. URL: https://linkinghub.elsevier.com/retrieve/pii/S1359835X13000730, doi:10.1016/j.compositesa.2013.03.002.

Lin, H., Wang, J., Long, A., Clifford, M., Harrison, P., 2007. Predictive modelling for optimization of textile composite forming. Composites Science

and Technology 67, 3242–3252. URL: https://linkinghub.elsevier.com/retrieve/pii/S026635380700156X, doi:10.1016/j.compscitech.2007.03.040.

Long, A.C., Rudd, C.D., 1994. A Simulation of Reinforcement Deformation during the Production of Preforms for Liquid Moulding Processes. Proceedings of the Institution of Mechanical Engineers, Part B: Journal of Engineering Manufacture 208, 269–278. URL: http://journals.sagepub.com/doi/10.1243/PIME_PROC_1994_208_088_02, doi:10.1243/PIME_PROC_1994_208_088_02.

Lukaszewicz, D.H.J., Ward, C., Potter, K.D., 2012. The engineering aspects of automated prepreg layup: History, present and future. Composites Part B: Engineering 43, 997–1009. URL: https://linkinghub.elsevier.com/retrieve/pii/S1359836811005452, doi:10.1016/j.compositesb.2011.12.003.

Madeo, A., Ferretti, M., dellIsola, F., Boisse, P., 2015. Thick fibrous composite reinforcements behave as special second-gradient materials: three-point bending of 3D interlocks. Zeitschrift fr angewandte Mathematik und Physik 66, 2041–2060. URL: http://link.springer.com/10.1007/s00033-015-0496-z, doi:10.1007/s00033-015-0496-z.

Mathieu, S., Hamila, N., Bouillon, F., Boisse, P., 2015. Enhanced modeling of 3D composite preform deformations taking into account local fiber bending stiffness. Composites Science and Technology 117, 322–333. URL: https://linkinghub.elsevier.com/retrieve/pii/S026635381530035X, doi:10.1016/j.compscitech.2015.07.005.

Meola, C., Boccardi, S., Carlomagno, G.m., 2017. Composite Materials in the Aeronautical Industry, in: Infrared Thermography in the Evaluation of Aerospace Composite Materials. Elsevier, pp. 1–24. URL: https://linkinghub.elsevier.com/retrieve/pii/B9781782421719000012, doi:10.1016/B978-1-78242-171-9.00001-2.

Middendorf, P., Metzner, C., 2011. Aerospace applications of non-crimp fabric composites, in: Non-Crimp Fabric Composites. Elsevier, pp. 441–449e. URL: https://linkinghub.elsevier.com/retrieve/pii/B9781845697624500187, doi:10.1533/9780857092533.4.441.

Mitchell, C.J., Dangora, L.M., Sherwood, J.A., 2016. Investigation into a robust finite element model for composite materials. Finite Elements in Analysis and Design 115, 1–8. URL: https://linkinghub.elsevier.com/retrieve/pii/S0168874X16300130, doi:10.1016/j.finel.2016.02.003.

Morley, L.S.D., 1971. The constant-moment plate-bending element. Journal of Strain Analysis 6, 20–24. URL: http://journals.sagepub.com/doi/10.1243/03093247V061020, doi:10.1243/03093247V061020.

Nguyen, Q., Vidal-Sall, E., Boisse, P., Park, C., Saouab, A., Brard, J., Hivet, G., 2013. Mesoscopic scale analyses of textile composite reinforcement compaction. Composites Part B: Engineering 44, 231–241. URL: https://linkinghub.elsevier.com/retrieve/pii/S135983681200354X, doi:10.1016/j.compositesb.2012.05.028.

Nishii, M., Hirashima, T., Kurashiki, T., 2014. Dry Fabric Forming

Analysis Considering the Influence of Tensions on In-plane Shear Behavior. Journal of the Society of Materials Science, Japan 63, 380–385. URL: http://jlc.jst.go.jp/DN/JST.JSTAGE/jsms/63.380?lang=en&from=CrossRef&type=abstract, doi:10.2472/jsms.63.380.

Oñate, E., Zárate, F., 2000. Rotation-free triangular plate and shell elements. International Journal for Numerical Methods in Engineering 47, 557–603. URL: http://onlinelibrary.wiley.com/doi/abs/10.1002/%28SICI%291097-0207%2820000110/30%2947%3A1/3%3C557%3A%3AAID-NME784%3E3.0.CO%3B2-9, doi:10.1002/(SICI)1097-0207(20000110/30)47:1/3<557::AID-NME784>3.0.CO;2-9.

Peng, X., Cao, J., 2005. A continuum mechanics-based non-orthogonal constitutive model for woven composite fabrics. Composites Part A: Applied Science and Manufacturing 36, 859–874. URL: https://linkinghub.elsevier.com/retrieve/pii/S1359835X04002593, doi:10.1016/j.compositesa.2004.08.008.

Potluri, P., Perez Ciurezu, D., Ramgulam, R., 2006. Measurement of meso-scale shear deformations for modelling textile composites. Composites Part A: Applied Science and Manufacturing 37, 303–314. URL: https://linkinghub.elsevier.com/retrieve/pii/S1359835X05002393, doi:10.1016/j.compositesa.2005.03.032.

Potluri, P., Sharma, S., Ramgulam, R., 2001. Comprehensive drape modelling for moulding 3D textile preforms. Composites Part A: Applied Science and Manufacturing 32, 1415–1424. URL: https://

linkinghub.elsevier.com/retrieve/pii/S1359835X01000409, doi:10.1016/S1359-835X(01)00040-9.

Rahali, Y., Giorgio, I., Ganghoffer, J., dell'Isola, F., 2015. Homogenization la Piola produces second gradient continuum models for linear pantographic lattices. International Journal of Engineering Science 97, 148–172. URL: https://linkinghub.elsevier.com/retrieve/pii/S0020722515001391, doi:10.1016/j.ijengsci.2015.10.003.

Sabourin, F., Brunet, M., 2006. Detailed formulation of the rotationfree triangular element S3 for general purpose shell analysis. Engineering Computations 23, 469–502. URL: https://www.emeraldinsight.com/doi/10.1108/02644400610671090, doi:10.1108/02644400610671090.

Sabourin, F., Vives, M., 2001. Elments finis triangulaires pour la simulation de l'emboutissage: Aspects de base. Revue Europenne des lments Finis 10, 7–53. URL: https://www.tandfonline.com/doi/full/10.1080/12506559.2001.11869238, doi:10.1080/12506559.2001.11869238.

Shin, C.M., Lee, B.C., 2014. Development of a strain-smoothed three-node triangular flat shell element with drilling degrees of freedom. Finite Elements in Analysis and Design 86, 71–80. URL: https://linkinghub.elsevier.com/retrieve/pii/S0168874X14000572, doi:10.1016/j.finel.2014.04.002.

Sjölander, J., Hallander, P., kermo, M., 2016. Forming induced wrinkling of composite laminates: A numerical study on wrinkling mechanisms. Composites Part A: Applied Science and Manufacturing

81, 41–51. URL: https://linkinghub.elsevier.com/retrieve/pii/S1359835X15003589, doi:10.1016/j.compositesa.2015.10.012.

Skordos, A., Monroy Aceves, C., Sutcliffe, M., 2007. A simplified rate dependent model of forming and wrinkling of pre-impregnated woven composites. Composites Part A: Applied Science and Manufacturing 38, 1318–1330. URL: https://linkinghub.elsevier.com/retrieve/pii/S1359835X06003046, doi:10.1016/j.compositesa.2006.11.005.

Soldatos, K.P., 2010. Second-gradient plane deformations of ideal fibre-reinforced materials: implications of hyper-elasticity theory. Journal of Engineering Mathematics 68, 99–127. URL: http://link.springer.com/10.1007/s10665-009-9353-4, doi:10.1007/s10665-009-9353-4.

Spencer, A., Soldatos, K., 2007. Finite deformations of fibre-reinforced elastic solids with fibre bending stiffness. International Journal of Non-Linear Mechanics 42, 355–368. URL: https://linkinghub.elsevier.com/retrieve/pii/S0020746207000686, doi:10.1016/j.ijnonlinmec.2007.02.015.

Tephany, C., Gillibert, J., Ouagne, P., Hivet, G., Allaoui, S., Soulat, D., 2016. Development of an experimental bench to reproduce the tow buckling defect appearing during the complex shape forming of structural flax based woven composite reinforcements. Composites Part A: Applied Science and Manufacturing 81, 22–33. URL: https://linkinghub.elsevier.com/retrieve/pii/S1359835X15003577, doi:10.1016/j.compositesa.2015.10.011.

ten Thije, R., Akkerman, R., Hutink, J., 2007. Large deformation simulation of anisotropic material using an updated Lagrangian finite element method. Computer Methods in Applied Mechanics and Engineering 196, 3141–3150. URL: https://linkinghub.elsevier.com/retrieve/pii/S0045782507000795, doi:10.1016/j.cma.2007.02.010.

Wang, J., Paton, R., Page, J., 1999. The draping of woven fabric preforms and prepregs for production of polymer composite components. Composites Part A: Applied Science and Manufacturing 30, 757–765. URL: https://linkinghub.elsevier.com/retrieve/pii/S1359835X98001870, doi:10.1016/S1359-835X(98)00187-0.

Willems, A., Lomov, S., Verpoest, I., Vandepitte, D., 2008a. Optical strain fields in shear and tensile testing of textile reinforcements. Composites Science and Technology 68, 807–819. URL: https://linkinghub.elsevier.com/retrieve/pii/S0266353807003405, doi:10.1016/j.compscitech.2007.08.018.

Willems, A., Lomov, S.V., Verpoest, I., Vandepitte, D., Harrison, P., Yu, W.R., 2008b. Forming simulation of a thermoplastic commingled woven textile on a double dome. International Journal of Material Forming 1, 965–968. URL: http://link.springer.com/10.1007/s12289-008-0218-6, doi:10.1007/s12289-008-0218-6.

Xue, P., Peng, X., Cao, J., 2003. A non-orthogonal constitutive model for characterizing woven composites. Composites Part A: Applied Science and Manufacturing 34, 183–193. URL: https://linkinghub.elsevier.

com/retrieve/pii/S1359835X02000520, doi:10.1016/S1359-835X(02)00052-0.

Yu, W.R., Harrison, P., Long, A., 2005a. Finite element forming simulation for non-crimp fabrics using a non-orthogonal constitutive equation. Composites Part A: Applied Science and Manufacturing 36, 1079–1093. URL: http://linkinghub.elsevier.com/retrieve/pii/S1359835X05000394, doi:10.1016/j.compositesa.2005.01.007.

Yu, W.R., Zampaloni, M., Pourboghrat, F., Chung, K., Kang, T.J., 2005b. Analysis of flexible bending behavior of woven preform using non-orthogonal constitutive equation. Composites Part A: Applied Science and Manufacturing 36, 839–850. URL: https://linkinghub.elsevier.com/retrieve/pii/S1359835X04002672, doi:10.1016/j.compositesa.2004.10.026.

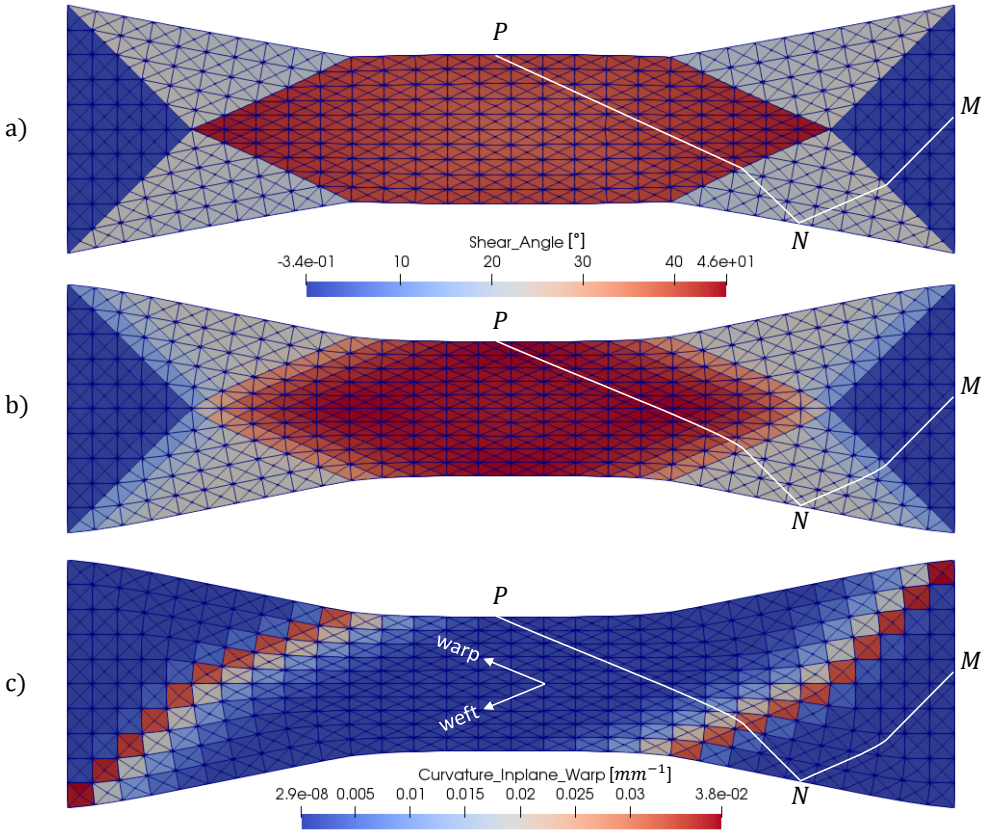

Figure 8: Bias-extension-test simulations with a 1200 elements mesh. (a) Shear angle field when simulated with negligeable in-plane bending rigidity ($k^{\chi} \simeq 0$) ; (b) Shear angle field when simulated with in-plane bending rigidity (table 1 properties) ; (c) Curvature field in warp direction.

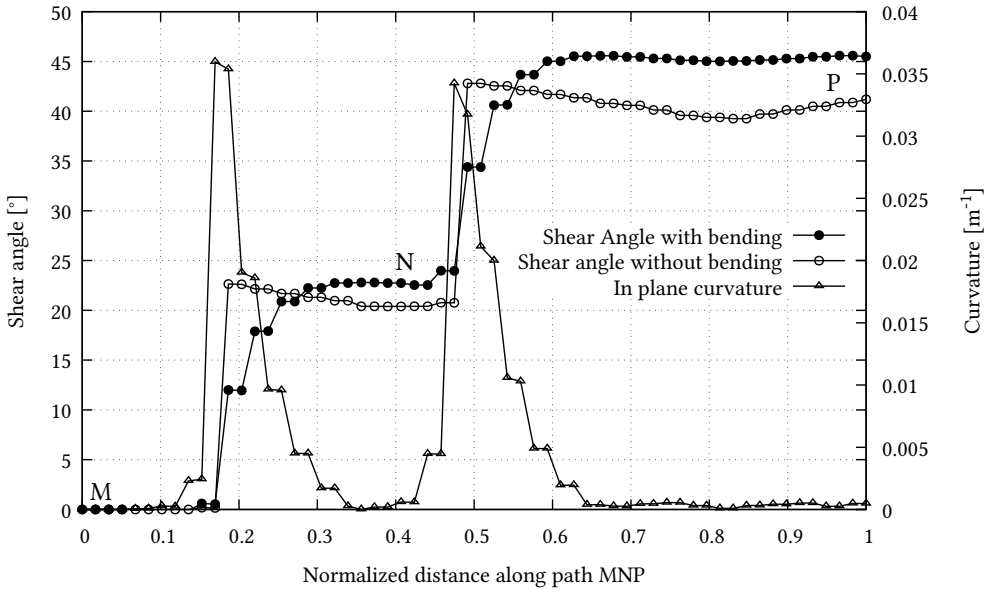

Figure 9: Shear angle and curvature along M-N-P path of Figure 8. For better reading, the dots M,N and P have been positioned approximately on the graph. Note that curvature is given in weft direction on M-N segment, and warp direction on N-P segment.

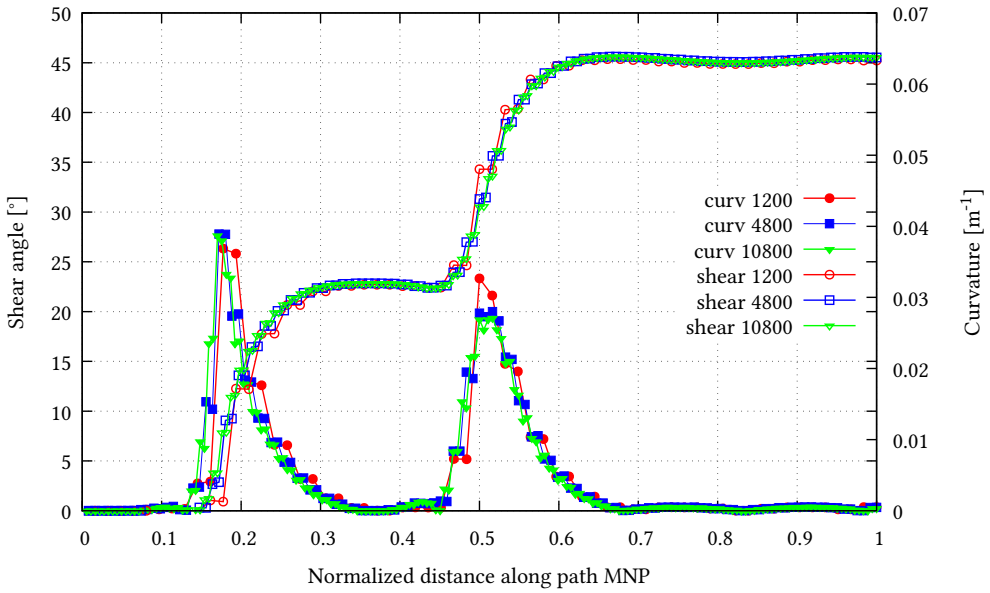

Figure 10: Shear angle and curvature along M-N-P path of Figure 8 for three different meshes containing 1200, 4800 and 10800 elements.

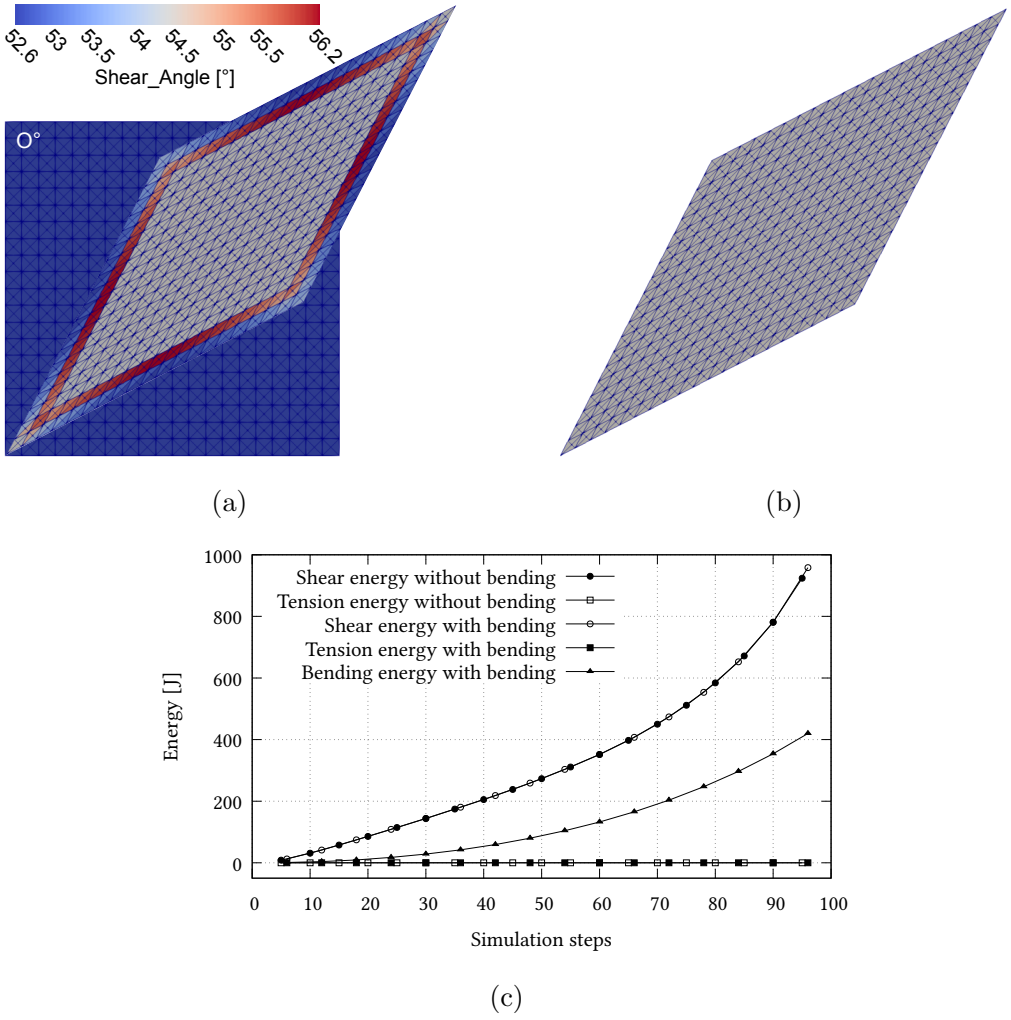

Figure 11: Picture frame simulation. (a) shear angle distribution accounting for in-plane bending rigidity; (b) shear angle distribution without in-plane bending rigidity (same color scale); (c) energetic contributions of tension, bending and shearing modes, with and without bending rigidity.

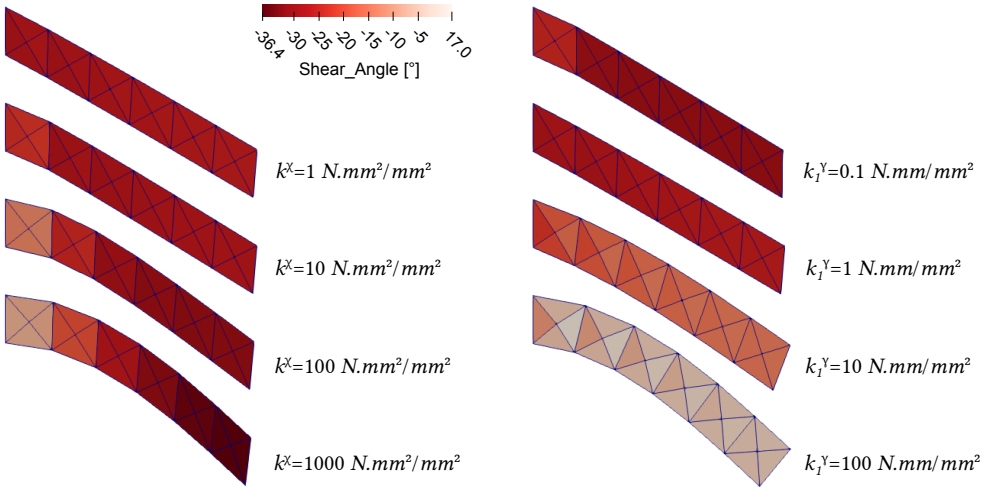

(a) $k_1^{\gamma} = 1N.mm/mm^2$ (b) $k^{\chi} = 1N.mm^2/mm^2$

Figure 12: cantilever bending simulation on a thick interlock with prescribed displacement; bending and shearing properties are modified independently.

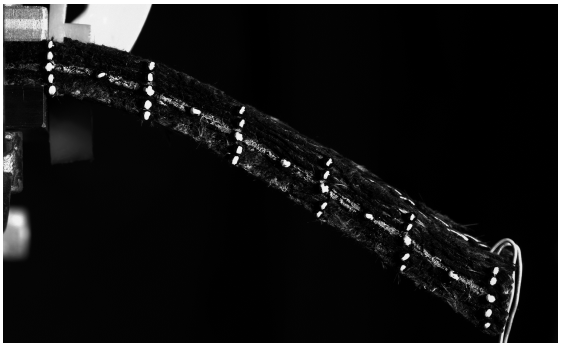

(a)

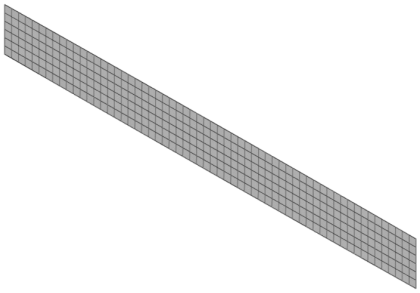

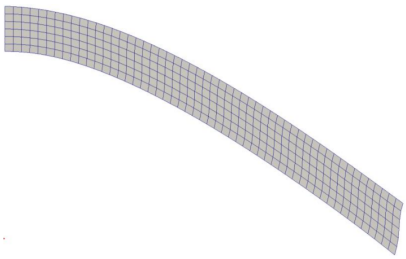

(b) (c)

Figure 13: Cantilever test on interlock sample $17 \times 50 \times 150\,\text{mm}$ with a 500 g suspended mass; (a) experimental result; (b) 1^{st} gradient solution in 3D finite element simulation; (c) enhanced 1^{st} gradient solution with shell element in middle plane.